Experimental Thermal and Fluid Science 62 (2015) 70–77

Contents lists available at ScienceDirect

Experimental Thermal and Fluid Science

journal homepage: www.elsevier.com/locate/etfs

Turbulent advances of a breaking bore: Preliminary physical experiments

Xinqian Leng, Hubert Chanson *

The University of Queensland, School Civil Engineering, Brisbane, QLD 4072, Australia

ARTICLE INFO

Article history:
Received 3 November 2014
Received in revised form 2 December 2014
Accepted 2 December 2014
Available online 10 December 2014

Keywords:
Breaking bore
Roller shape
Roller toe perimeter
Longitudinal roller profile
Roller toe elevation
Bore celerity
Air bubble entrainment
Jump toe
Turbulence
Physical modelling
Tidal bore

ABSTRACT

In an estuary, a tidal bore may be generated at the leading edge of the flood tidal wave during the early flood tide under spring tide conditions into a narrow funnelled channel. For Froude numbers greater than 1.4–1.6, the leading edge of the bore is characterised by a breaking roller. The roller is characterised by a sudden increase in water depth, a highly turbulent flow with large-scale vortical structures, some kinetic energy dissipation, a two-phase air–water flow region and strong turbulence interactions. New experiments were conducted in a large canal with a focus on breaking bore roller propagation. The upstream propagation of the roller toe was highly turbulent. The toe perimeter shape fluctuated rapidly with transverse distance and time. The celerity of the roller toe changed rapidly with time and space, although in a quasi-two-dimensional manner on average. The instantaneous longitudinal free-surface profile of the roller showed significant temporal and spatial fluctuations. New air–water flow measurements highlighted some distinctive air bubble entrainment at the toe of the roller. Bubbles with larger chord times were detected at higher vertical elevations in a more intermittent manner. Overall the study demonstrated that the propagation of breaking bore is a very turbulent, three-dimensional process.

1. Introduction

A sudden increase in flow depth in an open channel induces a positive surge [13,3,19]. In an estuary, a positive surge of tidal origin is called a tidal bore which may be generated by the early flood tide propagating upstream into a narrow funnelled channel under a large tidal range [34,8]. After formation, the bore may be analysed as a hydraulic jump in translation [30,20]. The shape of the surge front is a function of its Froude number Fr_1 [25,9]. For a rectangular channel, Fr_1 equals:

$$Fr_1 = \frac{V_1 + \overline{U}}{\sqrt{g \times d_1}} \quad (1)$$

where V_1 is the initial flow velocity positive downstream, $\overline{U}$ is the mean bore celerity positive upstream, g is the gravity acceleration, d_1 is the initial flow depth (Fig. 1A). For $Fr_1 > 1.4–1.6$, the leading edge of the bore is characterised by a breaking roller. Fig. 1B presents a photograph of a large breaking tidal bore in China. The bore roller is characterised by a sudden increase in water depth, a highly turbulent flow with large-scale vortical structures, some kinetic energy dissipation, a two-phase air–water flow region and strong turbulence interactions with the free surface associated with splashes and droplet ejections.

In this contribution, a physical investigation was conducted in laboratory with a focus on the bore roller properties. Detailed measurements were performed in a relatively large facility. The observations included a series of video observations of propagating breaking bores to characterise the roller toe perimeter, the bore front celerity and their fluctuations, as well as some preliminary unsteady air entrainment measurements in the bore roller using a dual-tip phase-detection probe. It is the purpose of this contribution to study thoroughly the upstream roller propagation and its turbulent fluctuations.

2. Experimental facility and instrumentation

New experiments were conducted in a 19 m long 0.7 m wide tilting channel, made of glass sidewalls and smooth PVC bed (Fig. 2). The bed slope was horizontal ($S_o = 0$) and the channel ended with a free overfall. The initially steady flow was supplied by a constant head reservoir, delivered into an upstream intake channel and led to the glass sidewalled test section through a

* Corresponding author. Fax: +61 7 33 65 45 99.
E-mail address: h.chanson@uq.edu.au (H. Chanson).
URL: http://www.uq.edu.au/~e2hchans/ (H. Chanson).

http://dx.doi.org/10.1016/j.expthermflusci.2014.12.002
0894-1777/

series of flow straighteners followed by a smooth bed and sidewall convergent. A fast-closing Tainter gate was located next to the test section's downstream end ($x = 18.1$ m), where x is the horizontal distance from the upstream end of the flume.

The video observations were conducted using a HD video camera Sony™ HDR-XR160, operating at 25 fps or 50 fps, with a resolution of 1920 × 1080 pixels, and a digital camera Casio™ Exlim EX-10, set at 120 fps (640 × 480 pixels), 240 fps (512 × 384 pixels) or 480 fps (224 × 160 pixels). The video camera was mounted vertically looking down across the channel width at about $x = 6.6$–6.7 m (Sony™ HDR-XR160) and $x = 9.2$ m (Casio™ Exlim EX-10). Fig. 2A illustrates a typical extract of video movies. A total of 15 videos were recorded under the same flow conditions, with 5 at 25 fps, 5 at 50 fps, 2 at 120 fps, 2 at 240 fps and 1 at 480 fps. A two-bulb fluorescent light was used to achieve a fast shutter speed. Photographic sequences in high-speed continuously shooting mode (8.3 fps) were taken through the sidewalls to capture the instantaneous free-surface profiles during the bore front passage (Fig. 2B). The dSLR camera was a Pentax™ K-3 (6016 × 4000 pixels) with Carl Zeiss™ Distagon 28 mm f2 lens, producing photographs with a low degree (<1%) of barrel distortion. Both the video movies and dSLR photographs were analysed manually to guarantee maximum reliability of the data.

During the air entrainment experiments, a dual-tip phase-detection conductivity probe was used to detect the bubbles entrained in the breaking roller. The sensor size was 0.25 mm and the longitudinal distance between the two tips was 6.5 mm. The dual-tip probe was excited by an electronic system (Ref. UQ82.518) designed with a response time of less than 10 μs. The vertical elevation of the probe was controlled by a Mitutoyo™ digimatic scale unit with an accuracy of 0.01 mm. The probe sampling rate was 40 kHz per sensor and the probe signal output was processed manually. The conductivity probe was placed at $x = 7.1$ m facing downstream and the measurements were performed at several elevations, typically above the initial water level. The data at different vertical elevations were synchronised using sideview photographs taken simultaneously, yielding the median free-surface elevations as a function of x–X, where X is the instantaneous roller toe longitudinal location.

For all experiments, the discharge was 0.085 m^3/s. The breaking bores were generated by the complete fast closure of the Tainter gate and the bore propagated upstream against the initially-steady flow (Fig. 2). Table 1 summarises the experimental flow conditions. Further details were reported in Leng and Chanson [18].

3. Basic results

3.1. Roller toe perimeter

In hydraulic jumps and breaking bores, the roller toe is a flow singularity where air is entrapped and vorticity is generated [14]. It is also called breaker foot [2] and corresponds to the position for base of a breaker, at the boundary between smooth and turbulent flow at the water surface, see the examples in Figs. 1B and 2. View in elevation, the roller toe formed a continuous line, herein called the roller toe perimeter (Fig. 1A). The shape of the roller toe perimeter and its evolution with time were investigated in details. For Runs 1, 2a and 4 (Table 1), the video movies were digitalised frame-by-frame to document the instantaneous perimeter of the roller toe during its upstream propagation and its variations with time. The data highlighted the broad range of instantaneous shapes of the roller toe perimeter. Fig. 3A shows typical instantaneous transverse profiles of the roller toe perimeter recorded at 120 fps, where $x = X$ is the instantaneous toe location at a transverse distance y with $y = 0$ at the left side wall. The roller toe was quasi two-dimensional on average, although its shape changed rapidly with both transverse direction and time. It is acknowledged that the finite width of the flume ($B = 0.7$ m) might affect the streamwise oscillation of the roller toe. The present data showed some backshifts of roller toe location with time, indicating that the toe occasionally shifted backwards for a very short time with a negative instantaneous celerity (e.g. Fig. 3, $t \approx 0.008$ & 0.149 s).

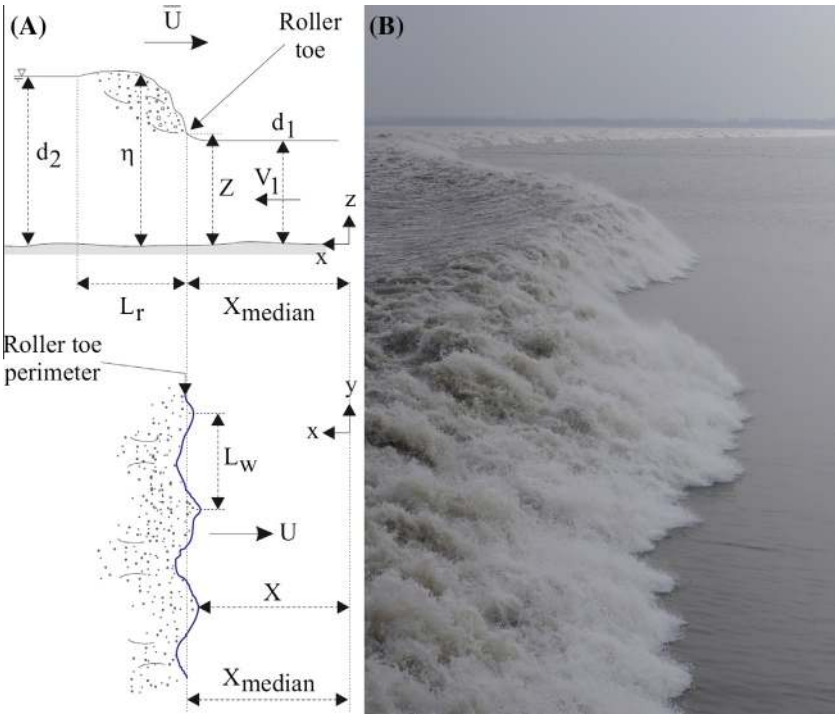

Fig. 1. Breaking bore. (A, Left) Definition ketch. (B, Right) Tidal bore of the Qiantang River (China) on 11 September 2014 between Yanguan and Laoyanchang (Shutter speed: 1/8000 s) – Bore propagation from left to right; the roller height was about 2–2.5 m and the bore celerity about 4 m/s.

(A) Photographic sequence with a time interval of 0.02 s photographs (Run 2a) - View in elevation with bore propagation from top to bottom

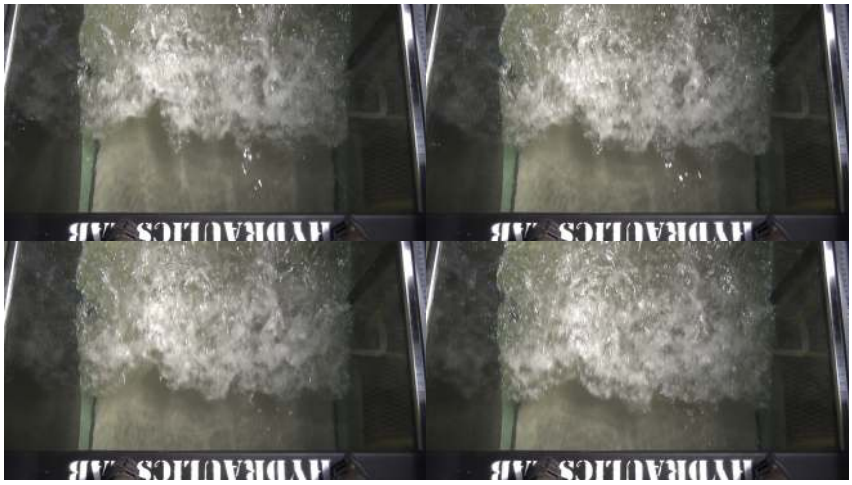

(B) Photographic side views of the bore roller with a time interval of 0.12 s between photographs (Run 3) - Bore propagation from left to right - Note the phase-detection probe on the top right

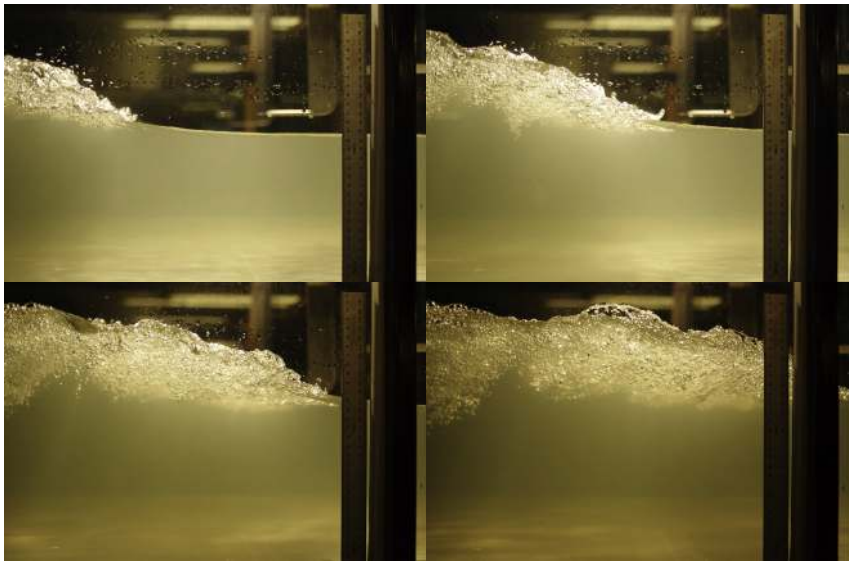

Fig. 2. Photographs of the experimental facility in operation.

The deviations of the roller toe perimeter about the instantaneous cross-sectional median position X_{median} were calculated, and the results indicated some quasi-periodic fluctuation of the toe perimeter in the transverse direction. A typical probability distribution function of transverse perimeter fluctuation $(X–X_{median})$ is shown in Fig. 3B. Overall the data sets exhibited a quasi-normal distribution and the results were basically independent of the movie frame rate, yielding $(X–X_{median})'/d_1 = 0.145$ on average at a given time, where $(X–X_{median})'$ is the standard deviation of the transverse perimeter fluctuation $(X–X_{median})$.

The transverse profile of the roller toe perimeter showed further some pseudo-periodic shape (Figs. 1 and 2A), indicating the existence of non-linear structures, streamwise vortices and streaks. This is also seen in Fig. 1B. At a fixed time, the fluctuations of toe perimeter location around its median were analysed in terms of relevant transverse wave lengths L_w, see definition in Fig. 1A. For the entire data set, the predominant transverse wave length was $L_w/d_1 \sim 1.2$. For comparison, Zhang et al. [38] reported transverse wave lengths of roller toe perimeters in stationary hydraulic jumps with wave lengths L_w/B between 2/3 and 2 where B is the channel width: that is, $13 < L_w/d_1 < 40$ for $Fr_1 = 6$. In the same study, a photograph suggested large streamwise vortices in the shear layer with wave lengths about $1–10 \times d_1$. Assuming a ratio of transverse to longitudinal wave lengths about 2/3 [1], this would correspond to dimensionless transverse wave lengths L_w/d_1 between 0.7 and 7. For completeness, Chanson [6] observed transverse integral turbulent length scales about $0.3 \times d_1$ in the developing air–water shear layer of stationary hydraulic jumps. The quantitative disparity between present data and strong hydraulic jump data is acknowledged. It is believed that this might be linked with a combination of effects, including the stationary nature of the hydraulic jumps, the very different Froude number range, and the difference in channel width which might reduce the streamwise oscillations in roller toe perimeter shapes. The former was discussed by Montes [24], Cointe [11] and Yeh and Mok [37], and further extended by Madsen [22] in the case of periodic bores. The effect of the Froude

Table 1
Experimental investigations of breaking bores.

References	Run	S_o	B (m)	Q (m^3/s)	d_1 (m)	V_1 (m/s)	$\overline{U}$ (m/s)	Fr_1	Instrumentation	Date
Present study	1	0	0.70	0.085	0.160	0.76	0.99	1.40	Video (25 fps) at x = 6.6 m	03/07/2014
	2a			0.085	0.146	0.83	0.95	1.49	Video (50 fps) at x = 6.6 m	09/07/2014
	2b			0.085	0.146	0.83	0.95	1.49	Phase-detection probe at x = 7.1 m	09/07/2014
	3			0.085	0.160	0.76	0.97	1.38	Phase-detection probe at x = 7.1 m	17/07/2014
	4			0.085	0.165	0.74	0.90	1.33	Video (120, 240, 480 fps) at x = 9.2 m	20/8/2014
Yeh and Mok [37]		0	0.61	0	0.060	0	–	1.35	Water sensors and argon-ion laser sheet	
					0.060	0	–	1.52		
					0.040	0	–	1.72		
					0.040	0	–	1.93		
					0.040	0	–	2.07		
Chanson [7]	091103	0	0.50	0.026	0.100	0.52	0.82	1.36	Hydrophone dolphin ear	3/11/2009
	091110b			0.043	0.138	0.63	0.95	1.36		10/11/2009
	091125			0.056	0.116	0.97	0.83	1.68		25/11/09
Docherty and Chanson [9]	Smooth	0	0.50	0.050	0.117	0.85	0.847	1.59	ADV, acoustic displacement meters	5/01/2010
	Gravel	0.002	0.50	0.050	0.127	0.79	0.885	1.50		19/01/2010
Chanson and Toi [10]	Smooth	0.0035	0.50	0.025	0.052	0.96	0.53	2.10	ADV, acoustic displacement meters	15/12/2010
	PVC				0.051	0.98	0.46	2.02		21/12/2010
					0.052	0.96	0.40	1.91		15/12/2010
					0.051	0.98	0.26	1.74		21/12/2010

Notes: B: channel width; d_1: initial water depth recorded at x = 7.1 m (Present study); Fr_1: bore Froude number: $Fr_1 = (\overline{U} + V_1)/(g \times d_1)^{1/2}$; S_o: bed slope; $\overline{U}$: cross-sectional time-averaged bore celerity recorded at x = 7.1 m (Present study); V_1: initial flow velocity recorded at x = 7.1 m (Present study); x: longitudinal distance from upstream end of glass sidewalled channel; (–): information not available.

(A) Instantaneous roller toe perimeter data - Bore propagation from top to bottom

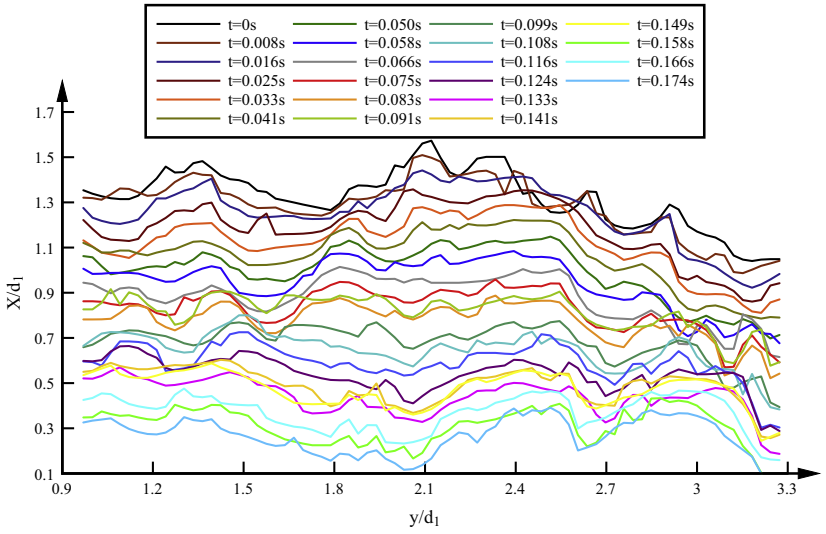

(B) Probability distributions functions of longitudinal fluctuations of roller toe about its median position

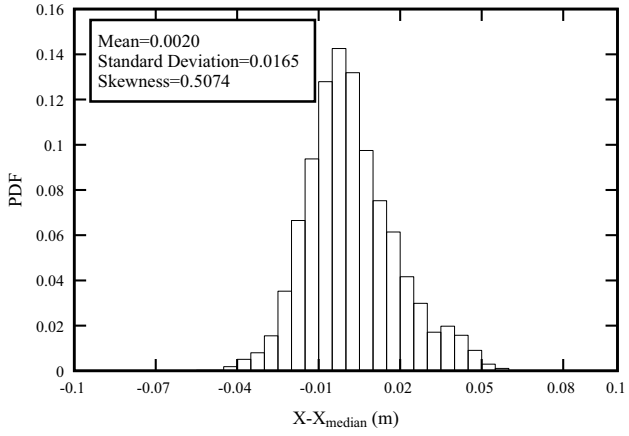

Fig. 3. Roller toe perimeter as function of transverse distance and time (Run 4, frame rate: 120 fps.

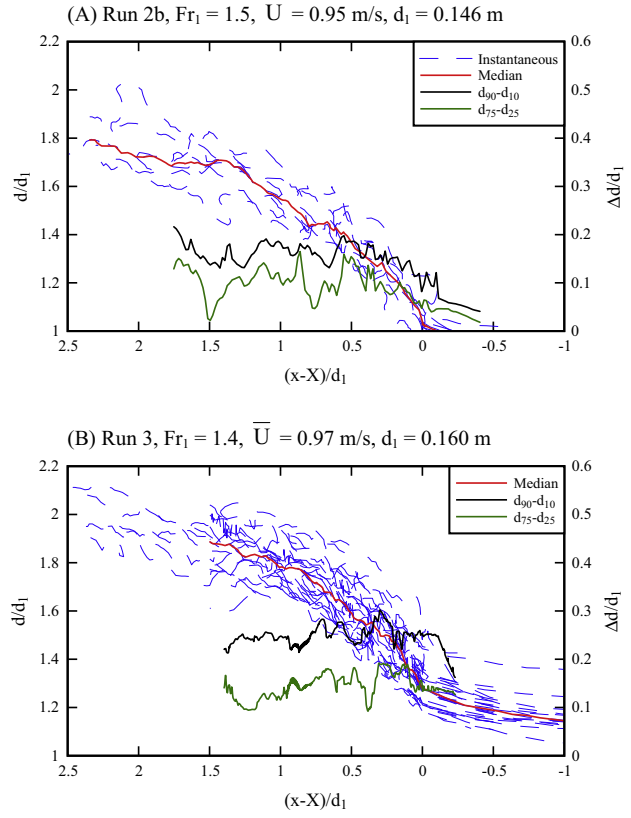

Fig. 4. Longitudinal roller profile of breaking bores – Instantaneous and median profiles, and free-surface fluctuations. (A) Run 2b, $Fr_1 = 1.5$, $\overline{U} = 0.95$ m/s, $d_1 = 0.146$ m. (B) Run 3, $Fr_1 = 1.4$, $\overline{U} = 0.97$ m/s, $d_1 = 0.160$ m

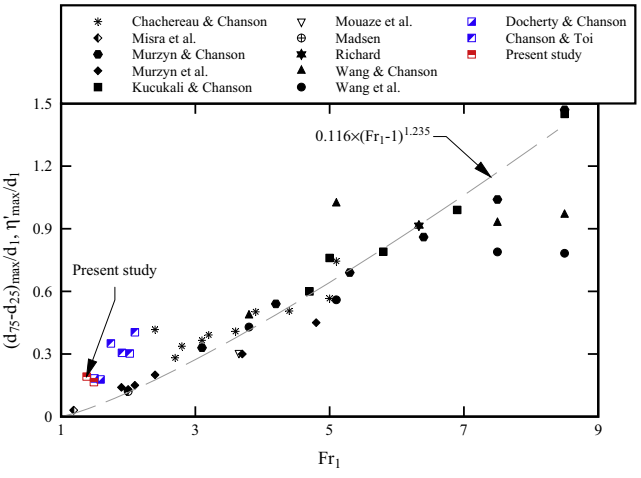

Fig. 5. Maximum free-surface fluctuations in breaking bores and hydraulic jumps as functions of Froude number – Tidal bore data: $(d_{75}–d_{25})_{max}/d_1$, Docherty and Chanson [12], Chanson and Toi [10], Present study (white and blue squares) – Hydraulic jump data η'_{max}/d_1: theoretical calculations [31], experimental data [22,26,23,27,17,28,4,35,36] (For interpretation of the references to colour in this figure legend, the reader is referred to the web version of this article.).

number was implicitly discussed by Hoyt and Sellin [15] and Long et al. [21]; their flow visualisations showed an increasing size of large vortical structures with increasing roller height and Froude number. Peregrine and Svendsen [29] argued that experimental data in strong hydraulic jumps might not be representative of bore characteristics.

3.2. Longitudinal roller profile

Typical instantaneous roller surface profiles are shown in Fig. 4, and Fig. 2B presents some photograph. Herein all longitudinal roller profiles were derived from high-shutter speed photographs taken through the left sidewall. All the data highlighted the rapid fluctuations in roller surface elevations as well as the rapid changes in longitudinal roller profiles with time. The instantaneous free-surface fluctuations were herein described in terms of the differences between 9th and 1st deciles ($d_{90}–d_{10}$) and third and first quartiles ($d_{75}–d_{25}$). For a Gaussian distribution of the data set about its mean, ($d_{90}–d_{10}$) and ($d_{75}–d_{25}$) would be equal respectively to 2.6 and 1.3 times the standard deviation [32]. The present data indicated a maximum in free-surface fluctuations in the first half of the roller (Fig. 4). The results $(d_{75}–d_{25})_{max}$ are reported in Fig. 5 and compared with the re-analyses of stationary hydraulic jump free-surface data sets which showed a marked maximum η'_{max} in turbulent fluctuations. Some re-analysed breaking tidal bore data are also included [12,10]. All the data showed free-surface fluctuations comparable between breaking bores and stationary hydraulic jumps for some comparable Froude number (Fig. 5). This is believed to be the first successful comparison of that kind.

The visual observations indicated that the free-surface elevation first rose slowly immediately prior to the roller for Froude numbers less than 2, as seen in Figs. 2B and 4. The gradual rise in free-surface ahead of the turbulent roller was previously observed [14,16]. Immediately after the roller toe, there was a marked discontinuity in the surface slope and curvature; the bore roller induced a sharp rise in water depth linked with the flow singularity (Fig. 4). The vertical elevation Z of the roller toe was recorded and the data were compared with re-analysed breaking bore data (Table 2). All the data showed a decrease in roller toe elevation, as well as a decrease in fluctuations in roller toe elevation, with increasing Froude number. The data were best correlated by:

$$\frac{Z_{median}}{d_1} - 1 = 0.1854 \times \exp\left(-3.52 \times (Fr_1 - 1.3)\right) \quad 1.3 < Fr_1 < 2 \tag{2}$$

$$\frac{Z_{75} - Z_{25}}{d_1} = 0.105 \times \exp\left(-1.99 \times (Fr_1 - 1.3)\right) \quad 1.3 < Fr_1 < 2 \tag{3}$$

where Z_{75} and Z_{25} are the third and first quartiles respectively. For $Fr_1 > 2$, the dimensionless roller toe elevation Z/d_1 tended to unity and the fluctuations in roller toe elevation tended to small values corresponding to the initial free-surface fluctuations.

3.3. Bore roller celerity

The bore roller celerity was derived from the instantaneous roller toe positions. The calculations were performed for seven transverse locations. The data showed no obvious sidewall effect, under the current experimental setup and for the flow conditions listed in Table 1. This was observed for all experiments and illustrated in Figs. 2A and 3. The results showed large fluctuations in bore celerity with the ratio of standard deviation to temporal mean U'/U_{mean}, about 1.0 on average. Yeh and Mok [37] reported similarly fluctuations in bore celerity, although with lesser fluctuation magnitudes. The instantaneous cross-sectional averaged celerity $\overline{U}$ was derived from the median roller perimeter data. The mean results are reported in Table 1 (column 9). Typical instantaneous data are presented in Fig. 6. In Fig. 6A, the instantaneous cross-sectional averaged celerity fluctuated rapidly with time about a median value of approximately $\overline{U} \approx 0.95$ m/s. The instantaneous celerity was not always positive, as seen for a few points in Fig. 6A. The negative celerity data were consistent with some

Table 2
Experimental observations of roller toe characteristics in breaking bores.

References	Bed	d_1 (m)	Fr_1	Measurement technique	$\frac{(d_{75}-d_{25})_{max}}{d_1}$	$\frac{Z_{median}}{d_1}$	$\frac{Z_{75}-Z_{25}}{d_1}$	Nb of data [a]
Present study	PVC	0.146	1.49	dSLR photography through sidewall	0.165	1.029	0.076	8
		0.160	1.38		0.192	1.166	0.109	29
Docherty and Chanson [9]	PVC	0.117	1.59	ADM measurements on centreline	0.178	1.063	0.043	25
	Gravel	0.127	1.50		0.183	1.107	0.043	25
Chanson and Toi (2015)	PVC	0.052	2.10	ADM measurements on centreline	0.404	1.008	0.017	10
		0.051	2.02		0.302	1.018	0.033	10
		0.052	1.91		0.305	1.032	0.045	10
		0.051	1.74		0.350	1.071	0.050	10

Notes: ADM: acoustic displacement meter; Fr_1: bore Froude number.
[a] Number of roller toe vertical elevation samples.

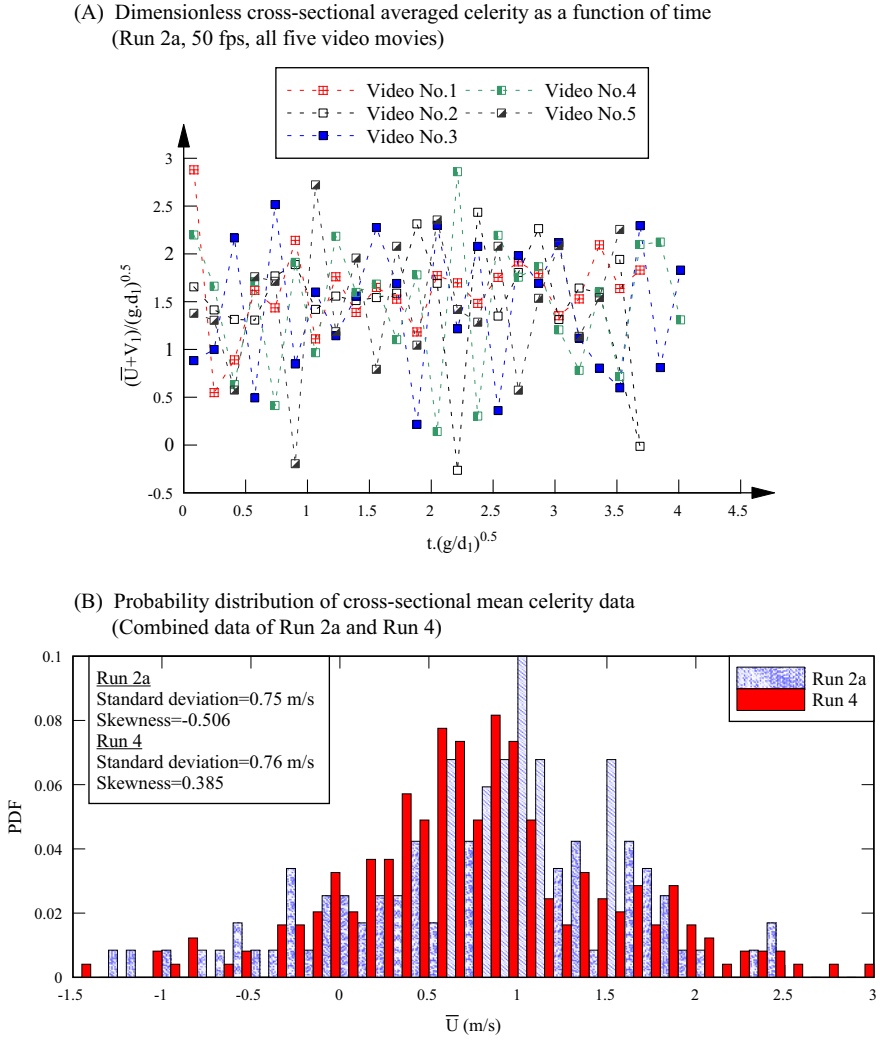

Fig. 6. Cross-sectional averaged celerity $\overline{U}$ of the bore roller toe.

intermittent backshift of the instantaneous roller toe perimeter discussed earlier. They might be related to the generation of turbulent vortices at the roller toe and their advection in the roller, as well as air bubble entrainment at the roller toe. Fig. 6B presents further the probability distribution function of the celerity $\overline{U}$. The data showed typically similar outcomes for video frame rates between 50 and 480 fps. The data at 25 fps tended to show some quantitative differences, likely caused by the sub-sampling.

4. Discussion: unsteady air bubble entrainment in the roller

The instantaneous void fraction c is defined as 0 in the water and 1 in the air. Fig. 7 presents the time variations of instantaneous void fraction c at different vertical elevation z/d_1, where t_{toe} is the time of passage of the bore roller toe. In Fig. 7, the black lines correspond to the leading tip probe signal and the red lines to the trailing sensor signal. The data showed consistently that a

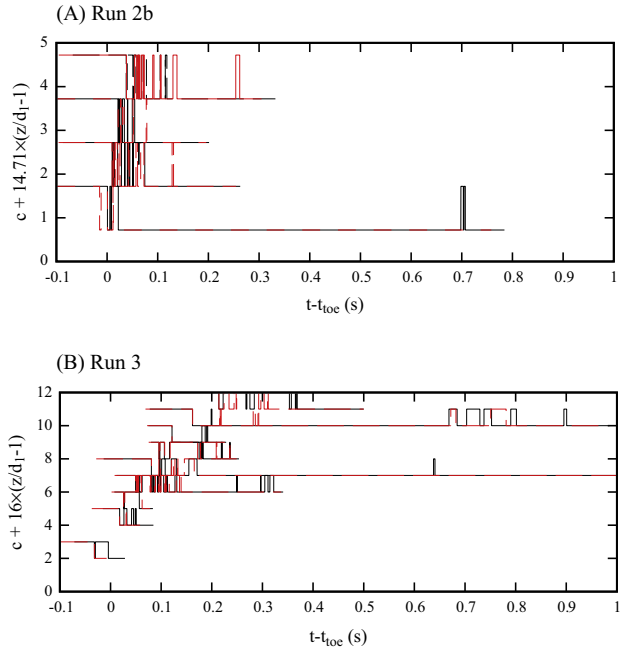

Fig. 7. Instantaneous void fraction c as a function of time (t–t_{toe}) at different vertical elevations above the initial flow depth – Black lines: leading tip signal; Red lines: trailing tip signal. (A) Run 2b. (B) Run 3. (For interpretation of the references to colour in this figure legend, the reader is referred to the web version of this article.)

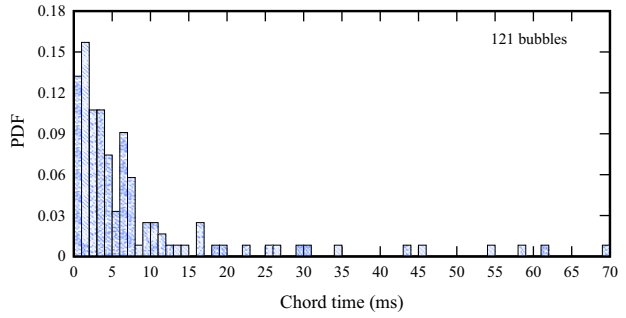

Fig. 8. Probability distribution functions of bubble chord times (Runs 2b & 3, all detected bubbles).

substantial number of bubbles were entrapped between $1.25 < z/d_1 < 1.5$. No bubble was detected for $z/d_1 < 1.05$, while, above $z/d_1 > 1.5$, the air entrainment was more intermittent and the probe sensor interacted with the upper free-surface. The arrival time of the first bubble was delayed with increasing elevation as predicted by the longitudinal roller profile (Fig. 7). In a few instances, the probe's leading tip was observed to detect the bore front after the trailing tip. This would be consistent with the bore roller interface moving with a negative celerity.

The bubble chord time data, recorded by both leading and trailing tips, showed increasing bubble chord times with increasing vertical elevations z/d_1. The largest number of bubbles were detected between $z/d_1 = 1.25$ and 1.5. Such a range of vertical elevations corresponded approximately to the impingement point (or roller toe) of the median bore front profile (Fig. 4). The probability distribution functions of bubble chord times at all vertical elevations are plotted in Fig. 8. Although the mean bubble chord time was 8.4 ms, the mode was about 2 ms and the data indicated a broad spectrum of chord times (Fig. 8). The present results were comparable to a previous study of stationary hydraulic jump for $Fr_1 = 3.1$ [5]. In that study, the large majority of detected bubbles had a chord time of 5 ms or less, with a mode about 1 ms. The present data showed also a small number of large bubble chord times (>20 ms), typically observed at higher elevations. There, the air entrainment was more intermittent, the probe sensor interacted with the upper free-surface, and both surface waves and surface roughness influenced significantly the chord time distributions, with an increased percentage of large chords [33].

High-shutter speed photographs showed a substantial number of bubbles with millimetric sizes: i.e., between 1 and 5 mm. Fig. 9 presents such a high-shutter speed photograph in which the two black squares have 2 mm sides. One such square is seen in the inset (Fig. 9, Right). The photographic observations were comparable to acoustic bubble size distributions recorded in breaking tidal bores (Table 1) [7]. This study recorded "acoustic" bubble radii between 0.4 and 14 mm. Although bubble sizes are not strictly comparable to bubble radii, present observations (Fig. 2B and 9) were of the same order of magnitude as acoustic bubble radii.

5. Conclusion

New experiments were conducted in a large flume to investigate breaking bores and the bore roller propagation. The results demonstrated several outcomes.

(1) The propagation of breaking bore roller toe was a highly turbulent process. Although the transverse shape of the roller toe perimeter was quasi two-dimensional on average, the toe perimeter shape fluctuated rapidly with transverse distance and time.

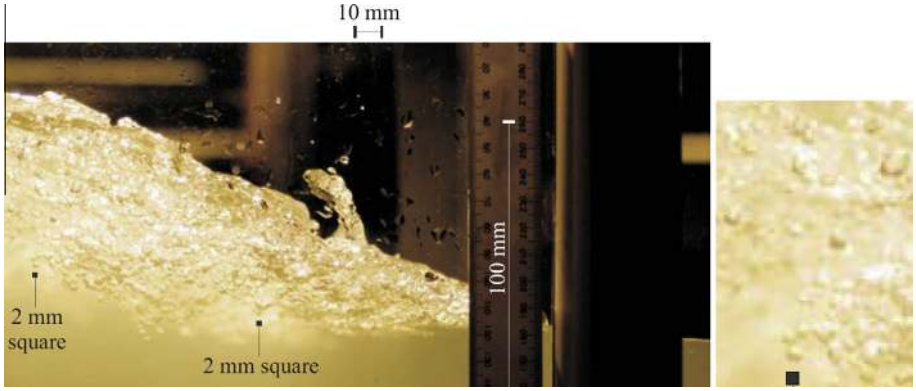

Fig. 9. Side view of the bore roller and entrained bubbles (shutter speed: 1/4000 s) (Run 3) – Bore propagation from left to right – Onset: details, with 2-mm black square for scale (bottom).

(2) The sidewalls had little effect on the upstream propagation of the breaking bore roller, within the experimental flow conditions.
(3) The celerity of the roller toe fluctuated rapidly with both time and transverse distance, although in a quasi-two-dimensional manner on average. Large fluctuations in bore celerity were observed, with U'/U_{mean}, about 1.0 on average. Instantaneous negative celerity data were infrequently recorded.
(4) The instantaneous longitudinal free-surface profile of the roller showed significant temporal and spatial fluctuations. The standard deviation of the free-surface elevation was maximum in the first half of the roller and the data were comparable to breaking tidal bore and stationary hydraulic jump data sets for a similar Froude number.
(5) For $Fr_1 < 2$, a gradual rise in free-surface was clearly observed ahead of the turbulent roller, and both the roller toe elevation and fluctuations in vertical elevation of roller toe decreased with increasing Froude number. The dimensionless roller toe elevation Z/d_1 tended to unity and the fluctuations in roller toe elevation tended to zero for $Fr_1 > 2$.
(6) The air–water flow measurements highlighted some distinctive air bubble entrainment at the toe of the roller. Bubbles with larger chord times were detected at higher vertical elevations in a more intermittent fashion, when the sensor interacted with the upper free-surface.

Altogether the study demonstrated that the propagation of breaking bore was a complicated turbulent process. The rapid fluctuations in roller toe perimeter and free-surface profiles indicated a strongly three-dimensional turbulent motion.

Acknowledgments

The authors thank Dr Frédéric MURZYN (ESTACA Laval, France) and Dr Hubert BRANGER (University of Aix-Marseille, France) for their detailed review of the report and very valuable comments. They also thank Professor Pierre LUBIN (University of Bordeaux, France) for his personal involvement, contribution and comments to the research project. They thank further both reviewers for their constructive and helpful comments. The authors acknowledge the technical assistance of Jason VAN DER GEVEL and Stewart MATTHEWS (The University of Queensland). The financial supports through the Australian Research Council (Grant DP120100481) and through the Agence Nationale de la Recherche (Projet MASCARET 10-BLAN-0911-01) are acknowledged.

References

[1] L.P. Bernal, A. Roshko, Streamwise vortex structure in plane mixing layers, J. Fluid Mech. 170 (1986) 499–525.
[2] M. Brocchini, D.H. Peregrine, The dynamics of strong turbulence at free surfaces. Part 2. Free-surface boundary conditions, J. Fluid Mech. 449 (2001) 255–290.
[3] A.E. Bryson, Film Notes for Waves in Fluids, Natl. Committee Fluid Mech. Films 21611 (1969) 8.
[4] Y. Chachereau, H. Chanson, Free-surface fluctuations and turbulence in hydraulic jumps, Exp. Thermal Fluid Sci. 35 (6) (2011) 896–909, http://dx.doi.org/10.1016/j.expthermflusci.2011.01.009.
[5] Y. Chachereau, H. Chanson, Bubbly flow measurements in hydraulic jumps with small inflow Froude numbers, Int. J. Multiph. Flow 37 (6) (2011) 555–564, http://dx.doi.org/10.1016/j.ijmultiphaseflow.2011.03.012.
[6] H. Chanson, Bubbly flow structure in hydraulic jump, Eur. J. Mech. B/Fluids 26 (3) (2007) 367–384, http://dx.doi.org/10.1016/j.euromechflu.2006.08.001.
[7] H. Chanson, The underwater noise of breaking tidal bores in laboratory, in: N.J. Docherty, H. Chanson, Characterisation of Unsteady Turbulence in Breaking Tidal Bores including the Effects of Bed Roughness, Hydraulic Model Report No. CH76/10, School of Civil Engineering, The University of Queensland, Brisbane, Australia, 2010, pp. 89–95.
[8] H. Chanson, Tidal Bores, Aegir, Eagre, Mascaret, Pororoca: Theory and Observations, World Scientific, Singapore, 2011, p. 220. ISBN 9789814335416.
[9] H. Chanson, Momentum considerations in hydraulic jumps and bores, J. Irrigation Drainage Eng. ASCE 138 (4) (2012) 382–385, http://dx.doi.org/10.1061/(ASCE)IR.1943-4774.0000409.
[10] H. Chanson, Y.H. Toi, Physical modelling of breaking tidal bores: comparison with prototype data, J. Hydraulic Res. IAHR, vol. XX (2015) (http://dx.doi.org/10.1080/00221686.2014.989458). (in print).
[11] R. Cointe, A theory of breakers and breaking waves, Ph.D. thesis, University of California, Santa Barbara, USA, 1987, 251 pages.
[12] N.J. Docherty, H. Chanson, Physical modelling of unsteady turbulence in breaking tidal bores, J. Hydraulic Eng., ASCE 138 (5) (2012) 412–419, http://dx.doi.org/10.1061/(ASCE)HY.1943-7900.0000542.
[13] F.M. Henderson, Open Channel Flow, MacMillan Company, New York, USA, 1966.
[14] H.G. Hornung, C. Willert, S. Turner, The flow field downstream of a hydraulic jump, J. Fluid Mech. 287 (1995) 299–316.
[15] J.W. Hoyt, R.H.J. Sellin, Hydraulic jump as 'Mixing Layer', J. Hyd. Eng., ASCE 115 (12) (1989) 1607–1614.
[16] C. Koch, H. Chanson, Turbulence measurements in positive surges and bores, J. Hydraulic Res., IAHR 47 (1) (2009) 29–40, http://dx.doi.org/10.3826/jhr.2009.2954.
[17] S. Kucukali, H. Chanson, Turbulence measurements in hydraulic jumps with partially-developed inflow conditions, Exp. Thermal Fluid Sci. 33 (1) (2008) 41–53, http://dx.doi.org/10.1016/j.expthermflusci.2008.06.012.
[18] X. Leng, H. Chanson, Turbulent advances of breaking bores: experimental observations, Hydraulic Model Report No. CH96/14, School of Civil Engineering, The University of Queensland, Brisbane, Australia, 2014, 40 pages. ISBN: 978 1 74272 130 9.
[19] J.A. Liggett, Fluid Mechanics, McGraw-Hill, New York, USA, 1994.
[20] J. Lighthill, Waves in Fluids, Cambridge University Press, Cambridge, UK, 1978. 504 pages.
[21] D. Long, N. Rajaratnam, P.M. Steffler, P.R. Smy, Structure of flow in hydraulic jumps, J. Hyd. Res., IAHR 29 (2) (1991) 207–218.
[22] P.A. Madsen, A model for a turbulent bore, Ph.D. thesis, Tech. Univ. of Denmark, Inst. of Hydrodynamics and Hyd. Eng., Copenhagen, Denmark, 1981, 149 pages. (also Series Paper No. 28, Tech. Univ. of Denmark, Inst. of Hydrodyamics and Hyd. Eng., Copenhager, Denmark, 149 pages.).
[23] S.K. Misra, M. Thomas, C. Kambhamettu, J.T. Kirby, F. Veron, M. Brocchini, Estimation of complex air–water interfaces from particle image velocimetry images, Exp. Fluids 40 (2006) 764–775, http://dx.doi.org/10.1007/s00348-006-0113-1.
[24] J.S. Montes, Undular hydraulic jump – discussion, J. Hyd. Div., ASCE 105 (HY9) (1979) 1208–1211.
[25] J.S. Montes, Hydraulics of Open Channel Flow, ASCE Press, New-York, USA, 1998. 697.
[26] D. Mouaze, F. Murzyn, J.R. Chaplin, Free surface length scale estimation in hydraulic jumps, J. Fluids Eng., ASME 127 (2005) 1191–1193.
[27] F. Murzyn, D. Mouaze, J.R. Chaplin, Air–water interface dynamic and free surface features in hydraulic jumps, J. Hydraulic Res., IAHR 45 (5) (2007) 679–685.
[28] F. Murzyn, H. Chanson, Free-surface fluctuations in hydraulic jumps: experimental observations, Exp. Thermal Fluid Sci. 33 (7) (2009) 1055–1064.
[29] D.H. Peregrine, I.A. Svendsen, Spilling breakers, bores and hydraulic jumps, in: A.D. Short (Ed.), Proc. of 16th International Conference on Coastal Engineering, ASCE, Hamburg, Germany, 1978, pp. 540–550 (Chapter 30).
[30] Lord Rayleigh, Note on tidal bores, Proc. Royal Soc. London, Ser A, Contain. Papers Math. Phys. Charact. 81 (541) (1908) 448–449.
[31] G. Richard, Élaboration d'un modèle d'écoulements turbulents en faible profondeur: Application au ressaut hydraulique et aux trains de rouleaux, ('Elaboration of a model of turbulent shallow water flows: Application to the hydraulic jump and roll waves.') Ph.D. thesis, University of Aix-Marseille, Institut Universitaire des Systèmes Thermiques Industriels IUSTI, France, 2013, 212 pages (in French).
[32] M.R. Spiegel, Theory and Problems of Statistics, McGraw-Hill Inc., New York, USA, 1972.
[33] L. Toombes, H. Chanson, Surface waves and roughness in self-aerated supercritical flow, Environ. Fluid Mech. 7 (3) (2007) 259–270, http://dx.doi.org/10.1007/s10652-007-9022-.
[34] R.A.R. Tricker, Bores, Breakers, Waves and Wakes, American Elsevier Publ. Co., New York, USA, 1965.
[35] H. Wang, H. Chanson, Free-surface deformation and two-phase flow measurements in hydraulic jumps, Hydraulic Model Report No. CH91/13, School of Civil Engineering, The University of Queensland, Brisbane, Australia, 2013, 108 pages (ISBN 9781742720746).
[36] H. Wang, F. Murzyn, H. Chanson, Total pressure fluctuations and two-phase flow turbulence in hydraulic jumps, Exp. Fluids 55 (11) (2014) 16, http://dx.doi.org/10.1007/s00348-014-1847-9. Paper 1847.
[37] H.H. Yeh, K.M. Mok, On turbulence in bores, Phys. Fluids A A2 (5) (1990) 821–828.
[38] G. Zhang, H. Wang, H. Chanson, Turbulence and aeration in hydraulic jumps: free-surface fluctuation and integral turbulent scale measurements, Environ. Fluid Mech. 13 (2) (2013) 189–204, http://dx.doi.org/10.1007/s10652-012-9254-3.